

**This is a self-archived version of an original article. This version may differ from the original in pagination and typographic details.**

**Author(s):** Sokołowska, Karolina; Luan, Zhongyue; Hulkko, Eero; Rameshan, Christoph; Barrabés, Noelia; Apkarian, Vartkess A.; Lahtinen, Tanja

**Title:** Chemically Selective Imaging of Individual Bonds through Scanning Electron Energy-Loss Spectroscopy : Disulfide Bridges Linking Gold Nanoclusters

**Year:** 2020

**Version:** Accepted version (Final draft)

**Copyright:** © 2020 American Chemical Society

**Rights:** In Copyright

**Rights url:** <http://rightsstatements.org/page/InC/1.0/?language=en>

**Please cite the original version:**

Sokołowska, K., Luan, Z., Hulkko, E., Rameshan, C., Barrabés, N., Apkarian, V. A., & Lahtinen, T. (2020). Chemically Selective Imaging of Individual Bonds through Scanning Electron Energy-Loss Spectroscopy : Disulfide Bridges Linking Gold Nanoclusters. *Journal of Physical Chemistry Letters*, 11(3), 796-799. <https://doi.org/10.1021/acs.jpcllett.9b03496>

Surfaces, Interfaces, and Catalysis; Physical Properties of Nanomaterials and Materials

## Chemically Selective Imaging of Individual Bonds Through Scanning Electron Energy-Loss Spectroscopy: Disulfide Bridges linking Gold Nanoclusters

Karolina Sokolowska, Zhongyue Luan, Eero Hulkko, Christoph Rameshan, Noelia Barrabes, Vartkess Ara Apkarian, and Tanja Lahtinen

*J. Phys. Chem. Lett.*, **Just Accepted Manuscript** • DOI: 10.1021/acs.jpcllett.9b03496 • Publication Date (Web): 15 Jan 2020

Downloaded from [pubs.acs.org](https://pubs.acs.org) on January 17, 2020

### Just Accepted

“Just Accepted” manuscripts have been peer-reviewed and accepted for publication. They are posted online prior to technical editing, formatting for publication and author proofing. The American Chemical Society provides “Just Accepted” as a service to the research community to expedite the dissemination of scientific material as soon as possible after acceptance. “Just Accepted” manuscripts appear in full in PDF format accompanied by an HTML abstract. “Just Accepted” manuscripts have been fully peer reviewed, but should not be considered the official version of record. They are citable by the Digital Object Identifier (DOI®). “Just Accepted” is an optional service offered to authors. Therefore, the “Just Accepted” Web site may not include all articles that will be published in the journal. After a manuscript is technically edited and formatted, it will be removed from the “Just Accepted” Web site and published as an ASAP article. Note that technical editing may introduce minor changes to the manuscript text and/or graphics which could affect content, and all legal disclaimers and ethical guidelines that apply to the journal pertain. ACS cannot be held responsible for errors or consequences arising from the use of information contained in these “Just Accepted” manuscripts.

1  
2  
3  
4  
5  
6  
7  
8  
9  
10  
11  
12  
13  
14  
15  
16  
17  
18  
19  
20  
21  
22  
23  
24  
25  
26  
27  
28  
29  
30  
31  
32  
33  
34  
35  
36  
37  
38  
39  
40  
41  
42  
43  
44  
45  
46  
47  
48  
49  
50  
51  
52  
53  
54  
55  
56  
57  
58  
59  
60

# Chemically Selective Imaging of Individual Bonds Through Scanning Electron Energy-Loss Spectroscopy: Disulfide Bridges linking Gold Nanoclusters

*Karolina Sokolowska,\*<sup>†</sup> Zhongyue Luan,<sup>‡</sup> Eero Hulkko,<sup>†,§</sup> Christoph Rameshan,<sup>||</sup> Noelia*

*Barrabés,<sup>||</sup> Vartkess A. Apkarian,<sup>⊥</sup> Tanja Lahtinen<sup>\*†</sup>*

<sup>†</sup>Department of Chemistry, Nanoscience Center, University of Jyväskylä, P.O. Box 35, 40014 Jyväskylä, Finland.

<sup>‡</sup>Department of Material Science and Engineering, University of California, Irvine, Irvine, CA 92697, USA.

<sup>§</sup>Department of Electronics and Nanoengineering, Aalto University, P.O. BOX 11000, FI-00076, Finland.

<sup>||</sup>Faculty of Technical Chemistry, Institute of Materials Chemistry, Technische Universität Wien, 1060 Vienna, Austria.

<sup>⊥</sup>Department of Chemistry, University of California, Irvine, Irvine, CA 92697, USA.

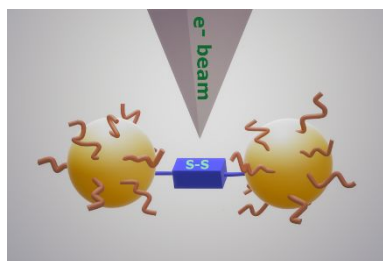
## AUTHOR INFORMATION

### Corresponding Authors

Email: [karolina.x.sokolowska@jyu.fi](mailto:karolina.x.sokolowska@jyu.fi); [tanja.m.lahtinen@jyu.fi](mailto:tanja.m.lahtinen@jyu.fi)

1  
2  
3 **As proof-of-principle of chemically selective, spatially resolved imaging of individual bonds,**  
4 **we carry out electron energy-loss spectroscopy (EELS) in a scanning transmission electron**  
5 **microscope (STEM) on atomically precise, thiolate-coated, gold nanoclusters linked with**  
6 **5,5'-bis(mercaptomethyl)-2,2'-bipyridine dithiol ligands. The images allow the identification**  
7 **of bridging disulfide bonds (R-S-S-R) between clusters and X-ray photoelectron spectra**  
8 **(XPS) support the finding.**  
9  
10  
11  
12  
13  
14  
15  
16  
17  
18  
19  
20

## 21 TOC GRAPHICS



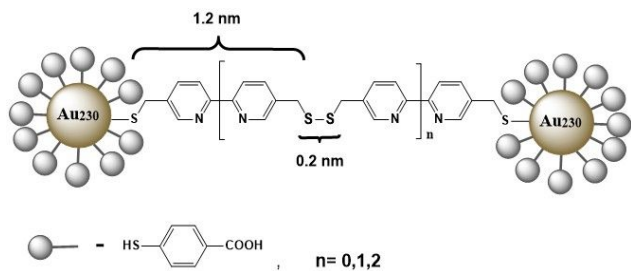
22  
23  
24  
25  
26  
27  
28  
29  
30  
31  
32  
33  
34 **KEYWORDS** Gold nanoclusters, linking, Electron energy-loss spectroscopy, X-ray  
35 photoelectron spectroscopy.  
36  
37  
38  
39  
40  
41  
42

43 Rapid progress is being made toward chemically selective atomically resolved microscopy, what  
44 may be regarded as the chemists' ideal structural tool. An example is the recent demonstration of  
45 imaging vibrational local modes inside a molecule through tip-enhanced Raman  
46 spectromicroscopy.<sup>1</sup> This involves measurements in the atomistic near-field, suitable for planar  
47 molecules. In contrast, the combination of scanning transmission electron microscopy (STEM)  
48 and electron energy-loss (EELS) microscopy provides a far-field method for chemically selective  
49  
50  
51  
52  
53  
54  
55  
56  
57  
58  
59  
60

1  
2  
3 atom-resolved spectromicroscopy, which has been implemented primarily to image the chemical  
4 structure of hard materials.<sup>2-5</sup> Its implementation in soft, organic materials has been limited due to  
5 the damage induced by the high energy electrons. With increasing detection sensitivity and energy  
6 resolution of electron analyzers, STEM-EELS can be expected to find wider use in direct chemical  
7 structure determination, where other methods may fail. We demonstrate this in the present, by  
8 imaging the disulfide-bridging bond between atomically precise, thiolate-coated gold  
9 nanoclusters, which was anticipated but could not be definitely established by standard  
10 spectroscopic means.

11  
12  
13  
14  
15  
16  
17  
18  
19  
20  
21  
22 Monolayer protected gold nanoclusters have attracted attention due to their physicochemical  
23 properties and applications such as surface chemical modification.<sup>6-9</sup> Of interest are gold  
24 nanoclusters with >200 gold atoms, which sustain localized surface plasmon resonances (LSPR)  
25 that can be tuned by modifying their immediate surroundings.<sup>10,11</sup> Modification of the nanocluster  
26 surface is necessary for assembly and implementations in biology, medicine or electronics.<sup>6,7,12</sup>  
27  
28  
29  
30  
31  
32  
33  
34  
35  
36  
37  
38  
39  
40  
41  
42  
43  
44  
45  
46  
47  
48  
49  
50  
51  
52  
53  
54  
55  
56  
57  
58  
59  
60

Ligand-exchange reactions are commonly used for this purpose, and bifunctional ligands are used to interconnect nanoclusters into superstructures with tunable optical and electronic properties.<sup>10,12-17</sup> The precisely-defined structural units and their ease in self-assembly allow systematic studies of emergent LSPR properties in individual superstructures, with the recognition that the linkage plays an important role in defining all such properties.<sup>18</sup> A predicate for such studies is the detailed knowledge of the chemical structure.



1  
2  
3 **Figure 1.** The suggested structure of two Au<sub>230</sub> nanoclusters linked by 5,5'-bis(mercaptomethyl)-  
4 2,2'-bipyridine (BMM-BPy) dithiols. Indicated are the lengths of the dithiol (1.2 nm), and the  
5  
6 disulfide bond (0.2 nm).  
7  
8  
9

10 We recently presented a versatile approach to covalently link Au<sub>210-230</sub>(*p*-MBA)<sub>70-80</sub> nanoclusters  
11 (Au<sub>230</sub>) into covalently linked dimers, trimers, and multimers.<sup>17</sup> Based on the analysis of reaction  
12 yields and Monte Carlo kinetic models, we speculated on reaction routes involving different  
13 linkages:<sup>19</sup> a single dithiol, or two to three dithiols fused by (-S-S-) disulfide bonds, as illustrated  
14 in Figure 1. This was indirectly supported by the observation of inter-cluster separations of 1 -  
15 2.85 times the length of a dithiol molecule.<sup>19</sup> However, conclusive spectroscopic proof could not  
16 be obtained through methods such as single-particle Raman, because of the spectral congestion by  
17 the thiolate-stapled gold clusters. To characterize the individual structures, it is necessary to  
18 combine high-resolution microscopy and high-sensitivity spectroscopy.<sup>2,3,20</sup> Electron microscopy  
19 has the capability to measure individual nanostructures.<sup>3,4,21,22</sup> STEM has previously been used to  
20 characterize the organic/inorganic, thiolate-protected gold nanoclusters on the sub-nanometer  
21 scale.<sup>4,22,23</sup> Here, to visualize the linkage, we employ EELS during STEM imaging, as previously  
22 implemented to study 2D materials and larger nanoparticles.<sup>3-5</sup> In addition, we exploit X-ray  
23 photoelectron spectroscopy (XPS) to provide complementary support.<sup>20</sup> The combination of these  
24 analytical tools allows the simultaneous structural and spectral analysis of individual  
25 nanostructures.  
26  
27  
28  
29  
30  
31  
32  
33  
34  
35  
36  
37  
38  
39  
40  
41  
42  
43  
44  
45  
46  
47  
48  
49  
50  
51  
52  
53  
54  
55  
56  
57  
58  
59  
60

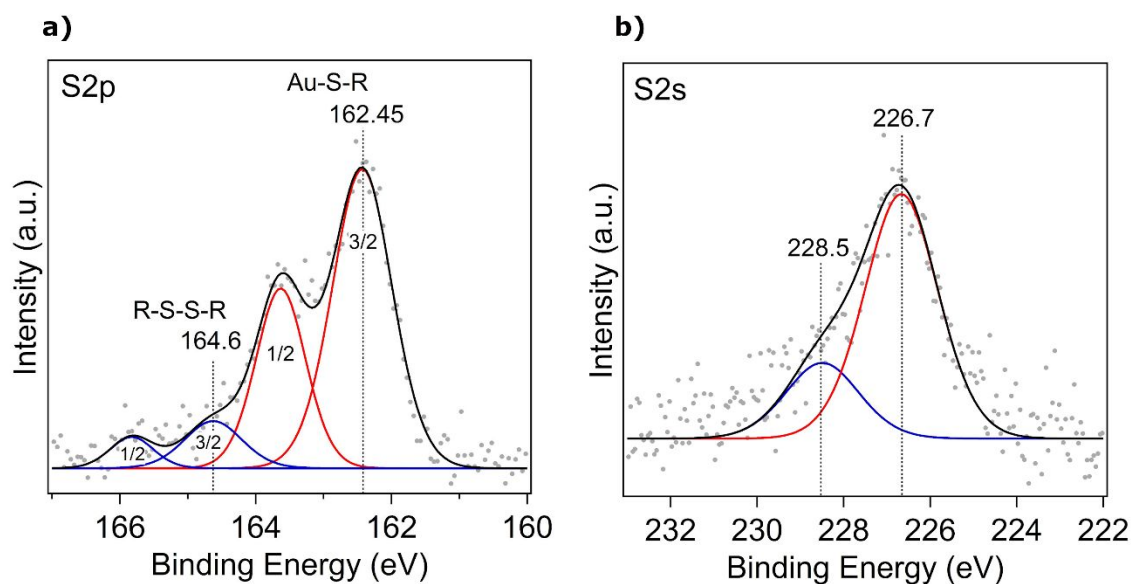


**Figure 2.** XPS of sulfur (a)  $2p$  and (b)  $2s$  spectra on  $\text{Au}_{230}$  linked oligomers. The  $2p$  signal is fitted to two spin-orbit split doublets  $2p_{1/2}$  and  $2p_{3/2}$ , and consistent with that, the  $2s$  spectrum is fitted to two peaks of the same relative intensity. The red peaks are assigned to S-Au and the blue peaks are assigned to S-S bound sulfur, respectively.

XPS allows elemental analysis of oligomers but lacks the sensitivity to pinpoint individual bonds (See SI experimental methods). The presence of gold, carbon, and a trace amount of oxygen is established through measurements of the core-level spectra of Au  $4f$ , C  $1s$ , and O  $1s$  (Fig. S1). The XPS core-level band around 84 eV is similar to bulk gold, with a linewidth (see Table S1) consistent with nanoclusters of approximately 4 nm in diameter.<sup>20</sup> In Fig. 2, we show the photoemission spectra of the S  $2p$  and S  $2s$  core-levels. The  $2p$  transition consists of spin-orbit split doublets and the spectrum in Fig. 2(a) shows two doublets. The red doublet with the  $2p_{3/2}$  component at 162.45 eV is assigned to the sulfur atoms chemically-bonded to gold atoms (S-Au). Similar binding energies at 162.6 eV,<sup>24</sup> 162.8 eV,<sup>25</sup> and 162.9 eV<sup>26</sup> have been observed before in

1  
2  
3 the thiolate-protected gold nanoclusters. The blue doublet, with  $2p_{3/2}$  component at 164.6 eV, is  
4  
5 admittedly weak. Confidence in this spectral decomposition is established by its consistency with  
6  
7 the S  $2s$  spectral profile shown in Fig. 2(b), which is best fitted to two peaks at 226.7 eV and 228.5  
8  
9 eV, with similar relative peak intensities as in the S  $2p$  doublet pair. The measured energy of the  
10  
11 blue doublet is in excellent agreement with the earlier work of Siegbahn and Verbist, where the  
12  
13 same signal at 164.6 eV was assigned to the disulfide group (R-S-S-R) that bridges dithiol  
14  
15 molecules.<sup>27</sup> As such, we assign the components at 162.5 eV and 164.6 eV in the S  $2p$  band, and  
16  
17 226.7 eV and 228.5 eV in the S  $2s$  band to S-Au and S-S bonded sulfur atoms, respectively. The  
18  
19 assignment establishes the presence of disulfide bonds but lacks the sensitivity to observe them in  
20  
21 individual covalently-linked clusters.  
22  
23  
24  
25

26 Aberration-corrected STEM images of a monomer, dimer, and trimer of  $Au_{230}$  clusters mounted  
27  
28 on a graphene-coated grid are shown in Fig. 3(a). The images are obtained at 80 kV, with current  
29  
30 and exposure time reduced to minimize e-beam damage, while retaining sufficient imaging  
31  
32 contrast. Close-ups of individual  $Au_{230}$  clusters are provided in Fig S2, where lattice fringes of  
33  
34  
35  
36  
37  
38  
39  
40  
41  
42  
43  
44  
45  
46  
47  
48  
49  
50  
51  
52  
53  
54  
55  
56  
57  
58  
59  
60



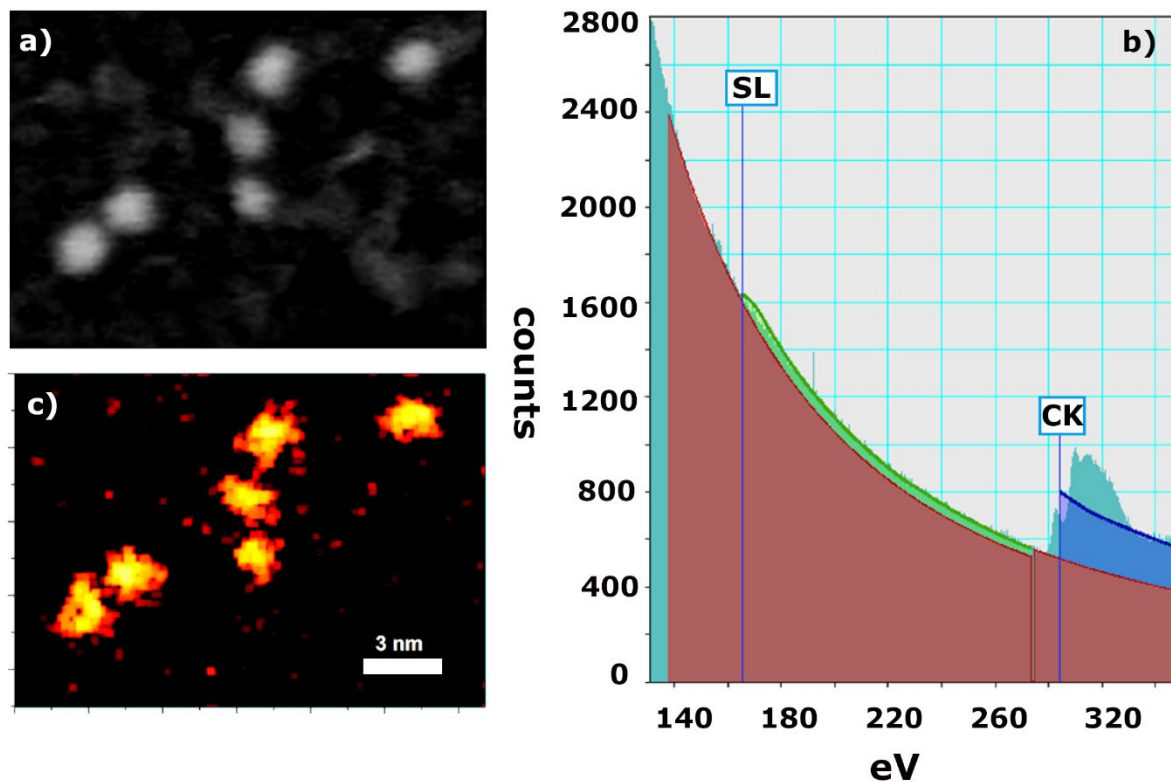


**Figure 3.** Atomic-level EELS mapping of covalently-linked gold oligomers: (a) STEM image, (b) EELS spectrum showing the opening of scattering channels at S L-edge and C K-edge, (c) Logarithmic intensity plot of the sulfur elemental map.

the face-centered-cubic arrangement can be seen, and the cluster diameter can be established as  $\sim 1.8$  nm, in agreement with our prior estimate of  $1.7 \pm 0.1$  nm.<sup>28</sup> The sample was prepared by dispersing a trimer solution purified by polyacrylamide gel electrophoresis (PAGE), however an overview of the dry-mounted clusters shows a wide distribution of superstructures (see Fig. S3). As earlier described,<sup>19</sup> dithiol-linked gold structures are dynamic in nature: they undergo continuous breaking and forming of superstructures. The EELS spectrum recorded under the same STEM imaging conditions is shown in Figure 3(b). In the core loss region  $>100$  eV, the spectrum shows the characteristic edges of sulfur (165 eV), carbon (284 eV) dominated by the graphene

1  
2  
3 grid, and trace amounts of nitrogen (401 eV) and oxygen (532 eV). The complete EELS spectrum  
4 is provided in Figure S4. The integrated S loss channel (highlighted in green in Fig. 3b) is mapped  
5 in Fig. 3(c) and Figure S5. The maps image the 70-80 sulfur atoms distributed on each  $\text{Au}_{210-230}(\text{p-}$   
6  $\text{MBA})_{70-80}$  cluster (close-ups provided in Fig. S6).

7  
8  
9  
10  
11  
12  
13  
14  
15 Line profiles of the elemental sulfur images in Figure 4 explore the inter-cluster bridges. The  
16 four images contain the variations seen (for close-ups, see Figs. S6 and S7). In Figs. 4(a) and (b),  
17 we see a clear intensity peak between the linked dimers, suggestive of a disulfide bond. Note, the  
18 pixel resolution is 0.16 nm, as such the two S atoms of the 0.2 nm-long S–S bond cannot be  
19 expected to be resolved. The intensity profile along the orange line in Fig. 4(c) is informative. It  
20 shows a peak between the first two clusters, similar to those in 4(a), (b). No such peak is found  
21 between the subsequent pairs. Indeed, the inter-cluster separation between clusters 2-3 and 3-4 of  
22  $\sim 1$  nm could only accommodate a single dithiol linker, and therefore a disulfide bond is not  
23 expected. The image of an isolated dimer bound by a single 1.2 nm dithiol, absent bridging sulfur,  
24 is provided in Fig. S8. In Fig. 4(d), we show the sulfur intensity profiles along with two-line cuts  
25 of a trimer. The orange line cuts across two nanoclusters, while the vertical cyan line passes  
26 through all three. The profile along the orange line is similar to those in Fig. 4(a) and (b), consistent  
27 with a disulfide linkage. The profile along the cyan line shows additional weak peaks  $\sim 0.5$  nm  
28 apart between nanoclusters separated by  $\sim 1.5$  nm, consistent with two disulfide bridges, therefore  
29 three dithiol molecules linking the two nanoclusters. In all cases, the intercluster separations are  
30 consistent with the expected number of dithiol linkers, and the visualized disulfide bonds, in full  
31 agreement with our prior hypothesis and finding on distances between nanoclusters (1- 2.85 times  
32 the length of BMM-BPy).

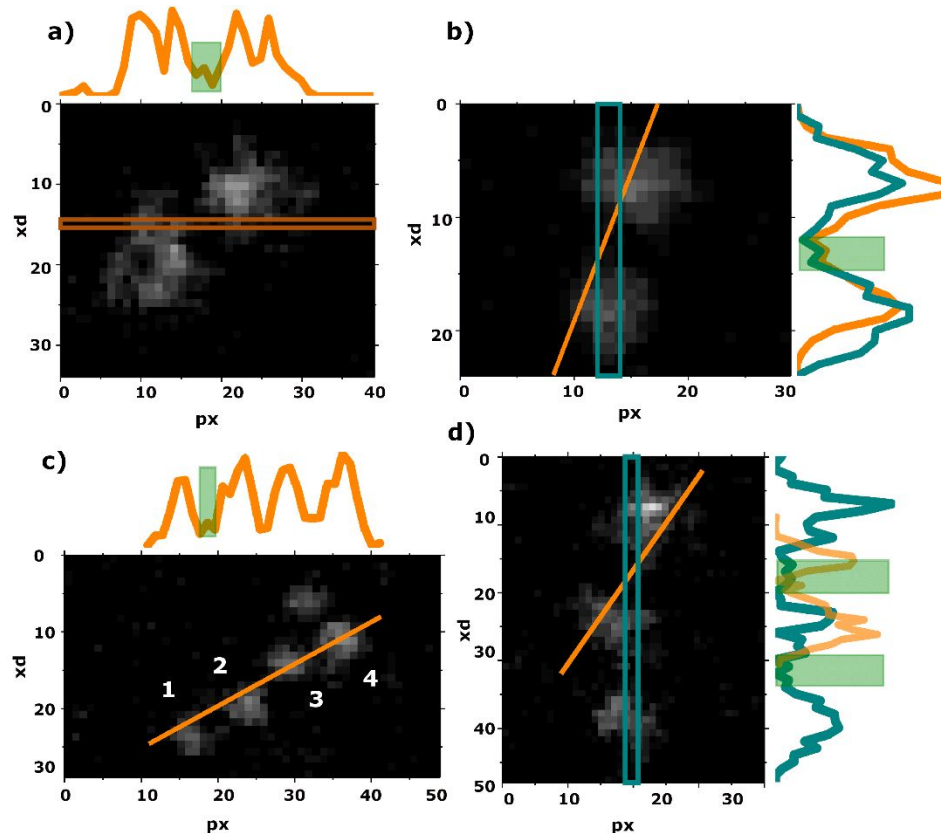


**Figure 4.** (a)—(d) The cross-section profiles of sulfur intensities taken along the lines indicated in the inset images. The inset images 4(a)—(d) are the same as the enlarged yellow-coded images shown in S5(a)—(d), respectively.

We have demonstrated that the combination of STEM and EELS already allows the visualization of chemical bonds and structure in real space. In the present implementation, we determined the disulfide linkages between dithiol-bound  $\text{Au}_{230}$  clusters, which to date was the subject of speculation. The nature and composition of the molecular bridges were also confirmed through XPS measurements. The combination of the three techniques provides comprehensive chemical analysis, which can be expected to have broader use as the resolution and sensitivity electron microscopies advance. The particular finding here, namely the bonding motif between

1  
2  
3 nanoclusters is important to advance our understanding of the optical and electronic response of  
4  
5 superstructures with emergent plasmonic response.  
6  
7

## 8 9 ASSOCIATED CONTENT

10  
11  
12 **Supporting Information.** The Supporting Information is available free of charge on the ACS  
13  
14 Publications website at DOI:

15  
16  
17  
18 Description of the experimental methods and measurements; Au 4*f*, C 1*s*, and O 1*s*  
19  
20 photoemission spectra along with the FWHM values; STEM micrographs of gold nanoclusters;  
21  
22 EELS spectrum of covalently-linked nanoclusters; intensity plot of sulfur elemental map derived  
23  
24 from EELS spectrum; cross-section profiles of sulfur intensities.  
25  
26  
27

## 28 29 AUTHOR INFORMATION

### 30 31 **Corresponding authors**

32  
33 \*K.B.S: E-mail: karolina.x.sokolowska@jyu.fi

34  
35 \*T.M.L: E-mail: tanja.m.lahtinen@jyu.fi

### 36 37 **ORCID**

38  
39 Eero Hulkko: 0000-0002-7536-5595

40  
41 Christoph Rameshan: 0000-0002-6340-4147

42  
43 Noelia Barrabés: 0000-0002-6018-3115

44  
45 Vartkess Ara Apkarian: 0000-0002-7648-5230

46  
47 Tanja Lahtinen: 0000-0002-1747-6959  
48  
49  
50  
51  
52  
53  
54  
55  
56  
57  
58  
59  
60

## Notes

The authors declare no competing financial interest.

## ACKNOWLEDGMENT

This work was supported by the National Science Foundation Center for Chemical Innovation on Chemistry at the Space-Time Limit (CaSTL), grant number CHE-1414466. STEM-EELS characterization was performed at the user facilities of the UC Irvine Materials Research Institute (IMRI), including instrumentation funded in part by the National Science Foundation Major Research Instrumentation Program under grant no. CHE-1338173. We thank Dr. Toshiro Aoki for support to measure STEM-EELS at IMRI and C.R. for providing XPS spectra. We acknowledge Zhipei Sun and Mika Pettersson for fruitful discussions and financial support.

## REFERENCES

- (1) Lee, J.; Crampton, K. T.; Tallarida, N.; Apkarian A.V. Visualizing Vibrational Normal Modes of a Single Molecule with Atomically Confined Light. *Nature*, **2019**, *568*, 78-82.
- (2) Römer, I.; Wang, Z. W.; Merrifield, R. C.; Palmer, R. E.; Lead, J. High-Resolution STEM-EELS Study of Silver Nanoparticles Exposed to Light and Humic Substances. *Environ. Sci. Technol.*, **2016**, *50*, 2183–2190.
- (3) Arenal, R.; De Matteis, L.; Custardoy, L.; Mayoral, A.; Tence, M.; Grazu, V.; De La Fuente, J. M.; Marquina, C.; Ibarra, M. R. Spatially-Resolved EELS Analysis of Antibody Distribution on Biofunctionalized Magnetic Nanoparticles. *ACS Nano*, **2013**, *7*, 4006–4013.

- 1  
2  
3 (4) Bahena, D.; Bhattarai, N.; Santiago, U.; Tlahuice, A.; Ponce, A.; Bach, S. B. H.; Yoon, B.;  
4 Whetten, R.L.; Landman, U.; Yacaman, M.J. STEM Electron Diffraction and High-  
5 Resolution Images Used in The Determination of the Crystal Structure of The Au<sub>144</sub>(SR)<sub>60</sub>  
6 Cluster. *J. Phys. Chem. Lett.*, **2013**, *4*, 975–981.  
7  
8  
9  
10  
11  
12  
13 (5) Koh, A. L.; Bao, K.; Khan, I.; Smith, W. E.; Kothleitner, G.; Nordlander, P.; Maier, S. A.;  
14 McComb, D. W. Electron Energy-Loss Spectroscopy (EELS) of Surface Plasmons in Single  
15 Silver Nanoparticles and Dimers: Influence of Beam Damage and Mapping of Dark Modes.  
16 *ACS Nano*, **2009**, *3*, 3015–3022.  
17  
18  
19  
20  
21  
22  
23 (6) Calard, F.; Wani, I. H.; Hayat, A.; Jarrosson, T.; Lère-Porte, J.-P.; Jafri, S. H. M.; Serein-  
24 Spirau, F.; Leifer, K.; Orthaber, A.; Designing Sterically Demanding Thiolate Coated AuNPs  
25 for Electrical Characterization of BPDT in a NP–Molecule–Nanoelectrode Platform. *Mol.*  
26 *Syst. Des. Eng.*, **2017**, *2*, 133–139.  
27  
28  
29  
30  
31  
32  
33 (7) Goswami, N.; Zheng, K.; Xie, J.; Bio-NCs – The Marriage of Ultrasmall Metal Nanoclusters  
34 with Biomolecules. *Nanoscale*, **2014**, *6*, 13328–13347.  
35  
36  
37  
38  
39 (8) Jin, R.; Zeng, C.; Zhou, M.; Chen, Y.; Atomically Precise Colloidal Metal Nanoclusters and  
40 Nanoparticles: Fundamentals and Opportunities. *Chem. Rev.*, **2016**, *116*, 10346-10413.  
41  
42  
43  
44 (9) Pezzato, C.; Maiti, S.; Chen, J. L.-Y.; Cazzolaro, A.; Gobbo, C.; Prins, L.J.; Monolayer  
45 Protected Gold Nanoparticles with Metal-Ion Binding Sites: Functional Systems for  
46 Chemosensing Applications. *Chem. Commun.*, **2015**, *51*, 9922-9931.  
47  
48  
49  
50  
51  
52 (10) Halas, N. J.; Lal, S.; Chang, W.-S.; Link, S.; Nordlander, P.; Plasmons in Strongly  
53 Coupled Metallic Nanostructures. *Chem. Rev.*, **2011**, *111*, 3913–3961.  
54  
55  
56  
57  
58  
59  
60

- 1  
2  
3 (11) Li, W.; Physics Models of Plasmonics: Single Nanoparticle, Complex Single Nanoparticle,  
4 Nanodimer, and Single Nanoparticle over Metallic Thin Film. *Plasmonics*, **2018**, *13*, 997–  
5 1014.  
6  
7  
8  
9  
10  
11 (12) Chakraborty, I.; Pradeep, T.; Atomically Precise Clusters of Noble Metals: Emerging Link  
12 between Atoms and Nanoparticles. *Chem. Rev.*, **2017**, *117*, 8208-8271.  
13  
14  
15  
16 (13) Azubel, M.; Kornberg, R.D.; Synthesis of Water-Soluble, Thiolate-Protected Gold  
17 Nanoparticles Uniform in Size. *Nano Lett.*, **2016**, *16*, 3348–3351.  
18  
19  
20  
21 (14) Compel, W. S.; Wong, O. A.; Chen, X.; Yi, C.; Geiss, R.; Häkkinen, H.; Knappenberger,  
22 K. L.; Ackerson, C. J.; Dynamic Diglyme-Mediated Self-Assembly of Gold Nanoclusters.  
23 *ACS Nano*, **2015**, *9*, 11690- 11698.  
24  
25  
26  
27  
28  
29 (15) Sels, A.; Salassa, G.; Cousin, F.; Lee, L.-T.; Bürgi, T.; Covalently Bonded Multimers of  
30 Au<sub>25</sub>(SBut)<sub>18</sub> As a Conjugated System. *Nanoscale*, **2018**, *10*, 12754–12762.  
31  
32  
33  
34  
35 (16) Jupally, V. R.; Kota, R.; Van Dornshuld, E.; Mattern, D.L.; Tschumper, G.S.; Jiang, D.-E.;  
36 Dass, A.; Interstaple Dithiol Cross-Linking in Au<sub>25</sub>(SR)<sub>18</sub> Nanomolecules: A Combined  
37 Mass Spectrometric and Computational Study. *J. Am. Chem. Soc.*, **2011**, *133*, 20258–20266.  
38  
39  
40  
41  
42 (17) Lahtinen, T.; Hulkko, E.; Sokołowska, K.; Tero, T.-R.; Saarnio, V.; Lindgren, J.;  
43 Pettersson, M.; Häkkinen, H.; Lehtovaara, L.; Covalently Linked Multimers of Gold  
44 Nanoclusters Au<sub>102</sub>(*p*-MBA)<sub>44</sub> and Au<sub>~250</sub>(*p*-MBA)<sub>n</sub>. *Nanoscale*, **2016**, *8*, 18665–18674.  
45  
46  
47  
48  
49  
50 (18) Malola, S.; Lehtovaara, L.; Enkovaara, J.; Häkkinen, H.; Birth of the Localized Surface  
51 Plasmon Resonance in Monolayer-Protected Gold Nanoclusters. *ACS Nano*, **2013**, *7*, 10263-  
52 10270.  
53  
54  
55  
56  
57  
58  
59  
60

- 1  
2  
3 (19) Sokołowska, K.; Hulkko, E.; Lehtovaara, L.; Lahtinen, T.; Dithiol-Induced  
4  
5 Oligomerization of Thiol-Protected Gold Nanoclusters. *J. Phys. Chem. C*, **2018**, *122*, 12524–  
6  
7 12533.  
8  
9  
10  
11 (20) Zhang, P.; X-ray Spectroscopy of Gold–Thiolate Nanoclusters. *J. Phys. Chem. C*, **2014**,  
12  
13 *118*, 25291–25299.  
14  
15  
16 (21) Vergara, S.; Lukes, D. A.; Martynowycz, M. W.; Santiago, U.; Plascencia-Villa, G.; Weiss,  
17  
18 S. C.; De La Cruz, M. J.; Black, D. M.; Alvarez, M. M.; López-Lozano, X.; et. al.; MicroED  
19  
20 Structure of Au<sub>146</sub>(*p*-MBA)<sub>57</sub> at Subatomic Resolution Reveals a Twinned FCC Cluster. *J.*  
21  
22 *Phys. Chem. Lett.*, **2017**, *8*, 5523–5530.  
23  
24  
25  
26 (22) Azubel, M.; Koh, A. L.; Koyasu, K.; Tsukuda, T.; Kornberg, R. D.; Structure  
27  
28 Determination of a Water-Soluble 144-Gold Atom Particle at Atomic Resolution by  
29  
30 Aberration-Corrected Electron Microscopy. *ACS Nano*, **2017**, *11*, 11866–11871.  
31  
32  
33  
34 (23) Azubel, M.; Koivisto, J.; Malola, S.; Bushnell, D.; Hura, G. L.; Koh, A. L.; Tsunoyama,  
35  
36 H.; Tsukuda, T.; Pettersson, M.; Häkkinen, H.; Kornberg, R.D.; Electron Microscopy of  
37  
38 Gold Nanoparticles at Atomic Resolution. *Science*, **2014**, *345*, 909–912.  
39  
40  
41  
42 (24) Gobbo, P.; Biesinger, M. C.; Workentin, M. S.; Facile Synthesis of Gold Nanoparticle  
43  
44 (AuNP)–Carbon Nanotube (CNT) Hybrids Through an Interfacial Michael Addition  
45  
46 Reaction. *Chem. Commun.*, **2013**, *49*, 2831–2833.  
47  
48  
49  
50 (25) Gobbo, P.; Mossman, Z.; Nazemi, A.; Niaux, A.; Biesinger, M. C.; Gillies, E. R.;  
51  
52 Workentin, M. S.; Versatile Strained Alkyne Modified Water-Soluble AuNPs  
53  
54  
55  
56  
57  
58  
59  
60



1  
2  
3 for Interfacial Strain Promoted Azide–Alkyne Cycloaddition (I-SPAAC). *J. Mater. Chem.*  
4 *B*, **2014**, *2*, 1764–1769.  
5  
6

7  
8 (26) Gobbo, P.; Novoa, S.; Biesinger, M. C.; Workentin, M. S.; Interfacial Strain-Promoted  
9 Alkyne–Azide Cycloaddition (I-SPAAC) for The Synthesis of Nanomaterial Hybrids. *Chem.*  
10 *Commun.*, **2013**, *49*, 3982–3984.  
11  
12  
13

14  
15 (27) Lindberg, B. J.; Hamrin, K.; Johansson, G.; Gelius, U.; Fahlman, A.; Nordling, C.;  
16 Siegbahn, K.; Molecular Spectroscopy by Means of ESCA II. Sulfur compounds. Correlation  
17 of electron binding energy with structure. *Phys. Scr.*, **1970**, *1*, 286–298.  
18  
19  
20  
21

22  
23 (28) Sokołowska, K.; Malola, S.; Lahtinen, M.; Saarnio, V.; Permi, P.; Koskinen, K.; Jalasvuori,  
24 M.; Häkkinen, H.; Lehtovaara, L.; Lahtinen, T.; Towards Controlled Synthesis of Water-  
25 Soluble Gold Nanoclusters: Synthesis and Analysis. *J. Phys. Chem. C*, **2019**, *123*, 2602–  
26  
27  
28  
29  
30  
31  
32  
33  
34  
35  
36  
37  
38  
39  
40  
41  
42  
43  
44  
45  
46  
47  
48  
49  
50  
51  
52  
53  
54  
55  
56  
57  
58  
59  
60